

**In-depth selectivity of the magnetic second-harmonic generation of light in a multilayer structure**L. C. Sampaio,\* J. Hamrle,<sup>†</sup> A. Mougin, and J. Ferré*Laboratoire de Physique des Solides, UMR CNRS 8502, Bat. 510, Université Paris-Sud, 91405 Orsay, France*

F. Garcia,\* F. Fettar, and B. Diény

*CEA Grenoble, Department de Recherche Fondamentale MC/SPINTEC and SP2M, 38043 Grenoble Cedex, France*

A. Brun

*Laboratoire Charles Fabri de l'Institut d'Optique Théorique et Appliquée, UMR CNRS 8501, Bat. 503, Université Paris-Sud, 91405 Orsay, France*

(Received 12 January 2004; revised manuscript received 9 April 2004; published 8 September 2004)

The in-depth selectivity of magneto-optical second-harmonic generation (MSHG) is investigated in the CoO/Co/NiO/Fe-Ni/Cu film structure. The  $p_{in}p_{out}$  MSHG is essentially selective to only one NiO/Fe-Ni buried magnetic interface, whereas  $p_{in}s_{out}$  and  $s_{in}p_{out}$  MSHG is shown to be magnetically sensitive to all interfaces. MSHG data are also compared to the usual longitudinal Kerr effect. Symmetry arguments and calculations point out that the observed in-depth MSHG selectivity is mainly linked to the electric field profile of the incident radiation through the multilayer structure.

DOI: 10.1103/PhysRevB.70.104403

PACS number(s): 75.25.+z, 75.60.-d, 75.70.Ak, 78.20.-e

**I. INTRODUCTION**

The use of pulsed lasers has opened up new possible investigations in science. High-power ultrashort pulses (100 fs or even shorter) allows the detection of nonlinear optical phenomena in particular media, i.e., harmonics of the fundamental ( $\omega$ ) excitation frequency. The second-harmonic generation (SHG) of light (at  $2\omega$ ) is of particular interest.<sup>1</sup> SHG originates from breaking of inversion symmetry, as found in noncentrosymmetric materials or at boundaries between two centrosymmetric media. Then, in a multilayer structure, SHG is emitted at the film surface or at each interface.<sup>1,2</sup>

For ferromagnetic (FM) materials, the radiated SHG intensity is dependent on the orientation of the sample magnetization.<sup>2-5</sup> This effect is called magnetization-induced second-harmonic generation (MSHG) of light, or sometimes nonlinear magneto-optical Kerr effect (NOMOKE or NOLIMOKE).<sup>2,5</sup> As for “classical” linear magneto-optical Kerr effect (MOKE) (i.e., both incident and detected light are at frequency  $\omega$ ), MSHG is due to two genuine quantum effects: the spin-orbit coupling and the exchange interaction. In thin magnetic film structures, both types of magneto-optical effects measure linear combinations of the magnetization components related to each layer.<sup>6</sup> While MOKE probes the entire volume of the multilayer with an in-depth reduced sensitivity,<sup>7</sup> MSHG is only selective to the magnetization of the film surface and of buried magnetic interfaces.<sup>2,5</sup>

Most MSHG measurements have been investigated so far on magnetic surfaces or on a sandwiched single magnetic layer, but only a few theoretical treatments and experiments have been devoted to magnetic multilayers.<sup>8-11</sup> The main reason is that the interpretation of MSHG data in multilayers becomes rapidly complex. However, convincing experiments are still required to show unambiguously how MSHG is related to the magnetic behavior of some buried interfaces in simple multilayer structures. Such a study is of particular interest for film structures that could be used in spintronics,

for example, to study the interfacial magnetic coupling in spin-valve or tunnel-junction structures. It has recently been used successfully to determine the reversible and irreversible parts of the magnetization at antiferromagnetic/ferromagnetic (AF/FM) interfaces in exchange-biased systems.<sup>10</sup>

The existing models fail to give a detailed interpretation of the MSHG data in simple magnetic multilayers. They often rely on crude (but sometimes justified) assumptions; for example, they consider nonabsorbing media.<sup>11</sup> In this paper, we propose the application of a more refined step by step treatment of SHG and MSHG based on light propagation inside a multilayer structure with  $2\omega$  emission at interfaces. MSHG in a magnetic multilayer structure is interpreted from selection rules related to the emission of light by dipoles at  $2\omega$  frequency and to their interface in-depth dependent sensitivity. We apply here our treatment to a tunnel-junction exchange-coupled structure with two different metallic FM layers (Fe-Ni and Co) separated by an AF oxide NiO layer. This structure shows a rich magnetic behavior<sup>12</sup> due to the interlayer exchange coupling of the FM layers across the AF spacer, giving rise to a spiraling spin structure in NiO. Such a type of system attracts great interest for potential applications in spintronics.

**II. GENERAL MSHG FORMALISM**

MSHG stands potentially as a promising technique for studying the magnetism of surfaces and buried interfaces in layered structures.<sup>2,5</sup> Let us summarize the main MSHG properties.

(i) As recalled in the Introduction, symmetry arguments indicate that MSHG is only allowed in noncentrosymmetric media. Then, in magnetic multilayers with centrosymmetric layer materials, MSHG probes only magnetism at the surface and at buried interfaces, for which the space inversion symmetry is broken.

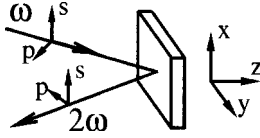


FIG. 1. Cartesian coordinate system used for the incoming and emitted light and for the direction of the applied field.

(ii) As for MOKE, MSHG measured in different optical polarization configurations can check any magnetization component.

(iii) The MOKE contributions coming from different FM layers are linearly additive.<sup>7,13</sup> The magnitudes of the MSHG contributions issued from different interfaces are additive as well, but provide a more complex behavior. For example, the phase of the SHG signal at the interface separating two metals changes sign when reversing the relative position of these metals.<sup>2</sup> Thus, a weakly absorbing ultrathin FM layer, sandwiched between non-magnetic layers composed with the same material, gives only rise to a very weak resultant MSHG signal.

Wierenga *et al.* have developed a formalism for calculating MSHG generated at interfaces of regular magnetic multilayer structures.<sup>14</sup> More recently, we proposed a more general formalism allowing to treat stacks of nonuniform magnetic layers,<sup>15</sup> based on the electric dipole emission mechanism at  $2\omega$  frequency. We summarize first the different stages (i)–(v) of the calculation, consistent with our formalism, and introduce pertinent  $\mathbf{X}_\nu^{(\omega)}$  and  $\mathbf{Z}_\nu^{(2\omega)}$  matrices.

(i) Assuming an isotropic interface, the electric field  $\mathbf{E}_\nu^{(\omega)}$  at the fundamental frequency  $\omega$  at each interface  $\nu$  is expressed within a matrix form,

$$\mathbf{E}_\nu^{(\omega)} = \mathbf{X}_\nu^{(\omega)} \mathbf{J}_0^{(\omega)}, \quad (1)$$

where  $\mathbf{X}_\nu^{(\omega)}$  is the matrix of incoming generalized Fresnel coefficients and  $\mathbf{J}_0^{(\omega)} = (\varepsilon_{s,0}^{(\omega)}, \varepsilon_{p,0}^{(\omega)})$  is the Jones vector of the incident electric field, with  $s, p$  the usual polarization states. In the considered Cartesian coordinate system, the  $z$  axis is oriented along the normal to the film plane, and  $y$  lies both in the planes of the film and of incidence (Fig. 1).

(ii) The electric field  $\mathbf{E}_\nu^{(\omega)}$  gives rise to electric point dipoles oscillating at frequency  $\omega$  with amplitude<sup>1,2</sup>

$$\boldsymbol{\mu}_\nu^{(2\omega)} = \chi_\nu \otimes \mathbf{E}_\nu^{(\omega)} \mathbf{E}_\nu^{(\omega)}, \quad (2)$$

where  $\chi_\nu$  is a third-rank susceptibility tensor. Depending upon the change of sign of the  $\chi_{ijk,\nu}$ 's elements with magnetization reversal, they can be classified as *nonmagnetic*  $\chi_{ijk,\nu}^{\text{nm}}(\mathbf{M}) = \chi_{ijk,\nu}^{\text{nm}}(-\mathbf{M})$ , or *magnetic*  $\chi_{ijk,\nu}^{\text{m}}(\mathbf{M}) = -\chi_{ijk,\nu}^{\text{m}}(-\mathbf{M})$  susceptibility tensor elements. Similarly, the electric dipole moment  $\boldsymbol{\mu}_\nu^{(2\omega)}$  can be separated into  $\boldsymbol{\mu}_\nu^{(2\omega)} = \boldsymbol{\mu}_\nu^{(2\omega)(\text{m})} + \boldsymbol{\mu}_\nu^{(2\omega)(\text{nm})}$ , where  $\boldsymbol{\mu}_\nu^{(2\omega)(\text{m})}$  and  $\boldsymbol{\mu}_\nu^{(2\omega)(\text{nm})}$  are the magnetic and nonmagnetic parts of the radiated electric point dipole, which change sign or not upon reversal of the magnetic field, respectively. Unfortunately, even considering symmetry arguments, the large number of nonzero susceptibility tensor elements  $\chi_{ijk,\nu}$  (see, e.g., Ref. 2) often makes their experimental determination difficult without crude assumptions.

Another limitation in the interpretation of the MSHG data comes from the difficulty to estimate the *active* SHG thickness around a given interface and that for all  $\chi_{ijk,\nu}$ 's. For an Al(111) surface, Pethukov and Liebsch<sup>16</sup> have calculated that SHG radiated by a normal current (i.e., by the normal dipole component  $\mu_z^{(2\omega)}$ ) is more surface sensitive than SHG radiated by tangential currents (i.e., by the tangential dipole components  $\mu_x^{(2\omega)}$  or  $\mu_y^{(2\omega)}$ ). This is also discussed by Gdde, Hohlfeld, and Matthias<sup>17</sup> in Co and Ni layers deposited on Cu. Then,  $\chi_{zzz}$  is found to be linked to sharp regions ( $\sim 0.1$  nm) located at interfaces, while  $\chi_{xxx}$  originates from a much thicker region expanding inside the magnetic layer ( $\sim 1$  nm). This physical argument is certainly valid in many other cases, as proved in the interpretation of our MSHG measurements on the Fe-Si/Dy-Fe-Co structure.<sup>27</sup>

(iii) The presence of a radiating point dipole  $\mu_\nu^{(2\omega)}$  at the  $\nu$ th interface implies modified boundary conditions of the radiated electric and magnetic field through this interface.<sup>15,18</sup> When all layers are assumed isotropic, the relation between  $\mu_\nu^{(2\omega)}$  and the outgoing electric field amplitudes  $\varepsilon_{\Pi,\nu}^{(2\omega)}$  at  $2\omega$  frequency (with  $\Pi = \{s, p\}$  are the light polarization states) is written

$$\begin{bmatrix} \varepsilon_{s,\nu}^{(2\omega)} \\ \varepsilon_{p,\nu}^{(2\omega)} \end{bmatrix} = \begin{bmatrix} Z_{sx,\nu}^{(2\omega)} & 0 & 0 \\ 0 & Z_{py,\nu}^{(2\omega)} & Z_{pz,\nu}^{(2\omega)} \end{bmatrix} \begin{bmatrix} \mu_{x,\nu}^{(2\omega)} \\ \mu_{y,\nu}^{(2\omega)} \\ \mu_{z,\nu}^{(2\omega)} \end{bmatrix}, \quad (3)$$

where  $\mathbf{Z}_\nu^{(2\omega)}$  stands for the matrix of generalized outgoing Fresnel elements. Here, we are determining the dipole radiation emitted inside the air superstrate. The zero coefficients in  $\mathbf{Z}_\nu^{(2\omega)}$  correspond to the fact that, inside the isotropic media, the  $\mu_{x,\nu}^{(2\omega)}$  component radiates only  $s$ -polarized waves, although  $\mu_{y,\nu}^{(2\omega)}$  and  $\mu_{z,\nu}^{(2\omega)}$  radiate  $p$ -polarized waves. It should be emphasized that the matrices  $\mathbf{X}_\nu^{(\omega)}$  and  $\mathbf{Z}_\nu^{(2\omega)}$  do not vary with sample magnetization when small contributions originating from Kerr and Faraday effects are neglected.

(iv) The resulting outgoing electrical field amplitudes  $\varepsilon_{\Pi,\text{tot}}^{(2\omega)}$  from the entire multilayer (denoted by the subscript tot) are then determined by a first integration over all radiating dipoles located on each interface, and second, by summing all interface contributions. When the magnetization and  $\chi_\nu$  of each interface is uniform,  $\varepsilon_{\Pi,\text{tot}}^{(2\omega)}$  is simply expressed by a sum over  $\varepsilon_{\Pi,\nu}^{(2\omega)}$ 's originating from one point dipole on each interface:<sup>15</sup>

$$\varepsilon_{\Pi,\text{tot}}^{(2\omega)} = \sum_\nu \varepsilon_{\Pi,\nu}^{(2\omega)}. \quad (4)$$

(v) The measured radiated SHG intensity in the far field is then given by<sup>15</sup>

$$I_{\text{tot}}^{(2\omega)} \sim |N_z^{(2\omega)}|^2 (|\varepsilon_{s,\text{tot}}^{(2\omega)}|^2 + |\varepsilon_{p,\text{tot}}^{(2\omega)}|^2), \quad (5)$$

where  $N_z^{(2\omega)} = \sqrt{(N^{(2\omega)})^2 - (N^{(\omega)} \sin \varphi)^2}$ ,  $\varphi$  being the incidence angle.  $N_z^{(\omega)}$  and  $N^{(2\omega)}$  are the refractive indices of the air at  $\omega$  and  $2\omega$ , respectively. In the particular case where  $N^{(\omega)} = N^{(2\omega)} = 1$ ,  $N_z^{(2\omega)}$  becomes equal to  $\cos \varphi$ .

TABLE I. Components of the SHG radiated dipole moment  $\mu_\nu^{(2\omega)}$  generated by the electric field  $\mathbf{E}_\nu^{(\omega)}$  at the  $\nu$ th interface, for various MSHG configurations and interface magnetization components. In order to simplify the notation, we omit the superscripts  $(2\omega)$  for  $\mu_\nu^{(2\omega)}$  and  $(\omega)$  for  $\mathbf{E}_\nu^{(\omega)}$  and the subscript  $\nu$ . As demonstrated in Sec. V, the contributions with underlines are dominant.

	Polar $M\parallel z$	Longitudinal $M\parallel y$	Transverse $M\parallel x$	Nonmagnetic
$p_{in}p_{out}$			$\mu_y = \chi_{yyy}^{(m)} E_y^2 + \chi_{yzz}^{(m)} E_z^2$ $\mu_z = \underline{\chi_{zzy}^{(m)}} E_y E_z$	$\mu_y = \chi_{yzy}^{(nm)} E_z E_y$ $\mu_z = \chi_{zyy}^{(nm)} E_y^2 + \chi_{zzz}^{(nm)} E_z^2$
$p_{in}s_{out}$	$\mu_x = \underline{\chi_{xzy}^{(m)}} E_y E_z$	$\mu_x = \underline{\chi_{xyy}^{(m)}} E_y^2 + \chi_{xzz}^{(m)} E_z^2$		
$s_{in}p_{out}$			$\mu_y = \underline{\chi_{yxx}^{(m)}} E_x^2$	$\mu_z = \chi_{zxx}^{(nm)} E_x^2$
$s_{in}s_{out}$		$\mu_x = \underline{\chi_{xxx}^{(m)}} E_x^2$		

MSHG is usually measured in four distinct optical configurations depending upon the polarization ( $s$  or  $p$ ) of the incoming (in) and outgoing (out) light beam. For example,  $p_{in}s_{out}$  means an incident  $p$ -polarized light for a detected  $s$ -polarized component (Fig. 1). Note that the  $s_{in}s_{out}$  configuration is usually not measured, since it gives a very weak MSHG signal. For a given optical configuration ( $p_{in}p_{out}$ ,  $s_{in}p_{out}$ ,  $p_{in}s_{out}$ , and  $s_{in}s_{out}$ ), the MSHG signal can be measured either in  $s_{out}$  out or  $p_{out}$  polarization, so that the total emitted light intensity  $I_{II,tot}^{(2\omega)(m)}$ , linear in magnetization, is

$$I_{II,tot}^{(2\omega)(m)} \sim 2|N_z^{(2\omega)}|^2 \sum_\nu \text{Re}[\epsilon_{II,\nu}^{(2\omega)(m)} (\epsilon_{II,tot}^{(2\omega)(nm)})^\dagger], \quad (6)$$

where the summation runs over all interfaces  $\nu$  and the dagger denotes the complex conjugate symbol.  $\epsilon_{II,tot}^{(2\omega)(nm)} = \sum_\nu \epsilon_{II,tot}^{(2\omega)(nm)}$  expresses the total *nonmagnetic* electric amplitude emitted by the sample.

Equation (6) shows that the magnetic part of the total radiated light intensity,  $I_{II,tot}^{(2\omega)(m)}$ , is simply given by a summation over contributions from all interfaces. Note that a contribution due only to the  $\nu$ th interface is determined by the product of the “magnetic” part of the electric field radiated by the  $\nu$ th interface by the *total* “nonmagnetic” part of the electrical field, originating from all interfaces. As follows from Eq. (6),  $I_{II,tot}^{(2\omega)(m)}$  is related to products  $\chi_\nu^{(nm)} \chi_\nu^{(m)}$  of nonlinear susceptibility tensor elements.<sup>1</sup>

Assuming an anisotropic interface, symmetry arguments allow nonmagnetic  $\chi_\nu^{(nm)}$  or magnetic  $\chi_\nu^{(m)}$  elements to be zero.<sup>2</sup> Consequently, the components of the radiating dipole  $\mu_\nu^{(2\omega)}$  only dependent upon particular components of the electric field  $\mathbf{E}_\nu^{(\omega)}$ . Their expressions are reported in Table I for different polarized light configurations ( $p_{in}p_{out}$ ,  $s_{in}p_{out}$ ,  $p_{in}s_{out}$ , and  $s_{in}s_{out}$ ) and magnetization components with respect to the light coordinate system (Fig. 1). Noting that, when rotating the sample by  $90^\circ$  around the  $\mathbf{z}$  axis the transverse magnetization becomes longitudinal, some  $\chi$  elements induced by a longitudinal magnetization are identical to others induced by a transverse magnetization. These relations are reported in Table II, for both magnetic and nonmagnetic  $\chi$  elements.

In this section, we have neglected other possible mechanisms that can give rise to MSHG. For example, structurally centrosymmetric media with nonuniform magnetization, occurring when magnetic domain walls are present, can theo-

retically give rise to MSHG via a term proportionnal to the gradient of the magnetization.<sup>2</sup> We can investigate this effect in our particular case of coupled FM films through an antiferromagnetic layer, where the interfacial coupling can obviously give rise to planar domain walls with nonuniform magnetization. This will not affect MSHG signals at magnetic saturation. Another contribution can come from the presence of antiferromagnetic interfaces; related MSHG effects have been predicted theoretically.<sup>19</sup> We shall address these points later in the final part of the discussion. Usually, these extra terms have a negligible contribution.

### III. SAMPLE PROPERTIES

The Co/NiO/Fe-Ni films were grown by sputtering in a high-vacuum chamber onto a thermally oxidized Si[100] substrate [SiO<sub>2</sub>(100 nm)/Si(0.5 mm)].<sup>12</sup> A Cu(5 nm) buffer layer was deposited first to promote a [111] texture and avoid a three-dimensional (3D) growth mode of Fe-Ni (more precisely Fe<sub>19</sub>N<sub>81</sub>, i.e., Permalloy) on SiO<sub>2</sub>. The polycrystalline AF NiO layer was deposited at oblique incidence by rf sputtering from a NiO target, while Co and Fe-Ni metallic layers were grown by dc sputtering at normal incidence. All depositions were performed at room temperature, in the absence of any applied magnetic field. The oblique sputtering procedure defines an easy in-plane AF uniaxial anisotropy in

TABLE II. Relationships between some magnetic and nonmagnetic  $\chi_{ijk}$  elements, resulting from symmetry arguments.

Transverse $\rightarrow$ Longitudinal
<b>Magnetic</b>
$\chi_{yzz}^{(m)} \rightarrow -\chi_{xzz}^{(m)}$
$\chi_{yxx}^{(m)} \rightarrow -\chi_{xyy}^{(m)}$
$\chi_{yyy}^{(m)} \rightarrow -\chi_{xxx}^{(m)}$
$\chi_{zzy}^{(m)} \rightarrow -\chi_{zzx}^{(m)}$
$\chi_{xxy}^{(m)} \rightarrow -\chi_{yxy}^{(m)}$
<b>Nonmagnetic</b>
$\chi_{zxx}^{(nm)} \rightarrow \chi_{zyy}^{(nm)}$
$\chi_{yzy}^{(cm)} \rightarrow \chi_{xzx}^{(cm)}$

NiO along a given  $\mathbf{c}$  axis. A weak ferromagnetic coupling or a  $90^\circ$  coupling between the two Co and Fe-Ni ferromagnetic layers are expected by choosing the NiO thickness equal to 8 or 4 nm, respectively.<sup>12</sup> We will discuss MSHG measured on both NiO(4 nm) or NiO(8 nm) films, keeping the same initial Fe-Ni and Co thickness of 10 and 4 nm, respectively. When exposed to ambient atmosphere, 1.5–2.0 nm of the top Co layer was oxidized into CoO. Note that this cobalt oxide is a paramagnetic insulator at room temperature and gives no magnetic contribution. Cross-section transmission electron microscopy and extended x-ray absorption fine-structure (EXAFS) measurements have also proved that an ultrathin ( $\sim 0.3$  nm) nonmagnetic oxidized CoO or Co-Ni-O layer is present at the Co/NiO interface.<sup>12</sup> Our film structure was finally CoO(2 nm)/Co(2 nm)/NiO(4 nm)/Ni-Fe(10 nm)/Cu(5 nm)/SiO<sub>2</sub>(100 nm)/Si.

As in the case of Fe-Ni/Fe-Mn/Co,<sup>20</sup> recent room-temperature data obtained on Co/NiO/Ni-Fe film structures<sup>12</sup> have clearly shown an in-depth spiraling spin structure for a thin enough NiO layer that is consistent with simulations.<sup>12</sup> In order to select a coupling between the two FM layers close to  $90^\circ$ , the NiO thickness must be about 4 nm and the anisotropies in our film structure have to verify the relations  $K_{\text{Co}} > K_{\text{NiO}} \gg K_{\text{Fe-Ni}}$ . Reasonable values of the anisotropy constants are  $K_{\text{Co}} = 5 \times 10^5$  erg/cm<sup>3</sup>,  $K_{\text{NiO}} = 4 \times 10^4$  erg/cm<sup>3</sup>,  $K_{\text{Fe-Ni}} \sim 0$ .<sup>12</sup> Driven by our selective preparation conditions, the Co, Fe-Ni, and NiO layers have the same in-plane magnetic easy anisotropy axis  $\mathbf{c}$ . The magnetization of the Co layer in zero field always lies along the  $\mathbf{c}$  axis, but as in Fe/NiO/Co film structures,<sup>21</sup> the  $90^\circ$  coupling, driven by the combined effect of a propagating nearest coupling in the AF NiO spacer and interface roughness, tends to orient the Fe-Ni magnetization towards the normal to the  $\mathbf{c}$  axis, which is consistent with simulations.<sup>12</sup> Contrastingly, with other structures showing the same behavior,<sup>21,22</sup> our nonsymmetric structures, with hard (Co) and soft (Fe-Ni) FM layers, allow us to distinguish the magnetic and MSHG behaviors of the two FM layers.

#### IV. EXPERIMENTAL RESULTS

Longitudinal ( $\parallel \mathbf{y}$ ) (Fig. 1) LMOKE hysteresis loops have been measured by a modulation technique.<sup>23</sup> The field was applied along the Co easy anisotropy  $\mathbf{c}$  axis. Figure 2 shows such LMOKE hysteresis loops for the NiO(8 nm) and NiO(4 nm) films. For the NiO(8 nm) film [Fig. 2(a)], the resulting loop is a superposition of two square loops due to the Fe-Ni ( $H_C \sim 13$  Oe) and Co ( $H_C \sim 220$  Oe) layers. This proves that the magnetization of the Fe-Ni and Co layers are nearly aligned with the  $\mathbf{c}$  axis. For the NiO(4 nm) film [Fig. 2(b)], the data differ markedly since the loop results in a superposition of a Co square loop with a rather large coercivity ( $H_C \sim 170$  Oe), and a field-induced S-shape contribution related to the quasireversible spin reorientation in the Fe-Ni layer. This confirms that, for the NiO(4 nm) film, the magnetization of the Fe-Ni layer is coupled at about  $90^\circ$  in zero field from the Co magnetization.<sup>12</sup> Nevertheless, the Fe-Ni minor loop [inset of Fig. 2(b)] shows hysteresis and an

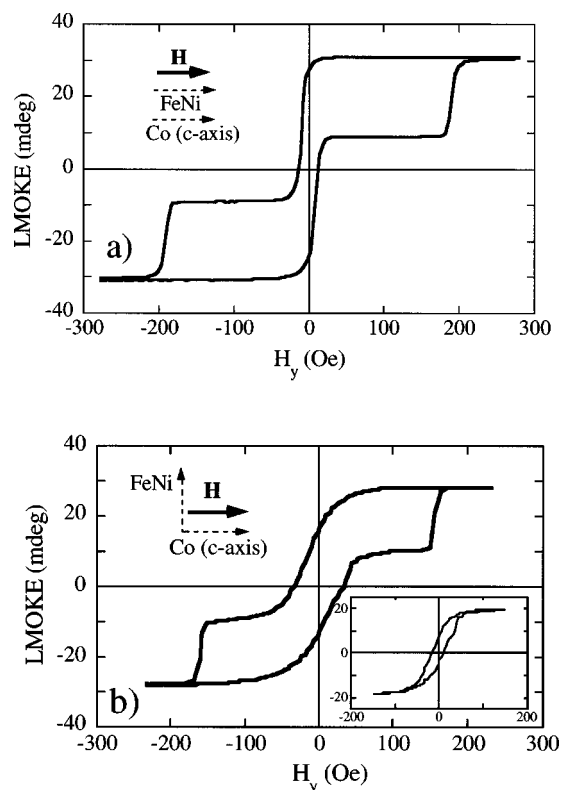


FIG. 2. Longitudinal LMOKE loops measured for  $\mathbf{H} \parallel \mathbf{c}$  in: (a) the NiO(8 nm) film, (b) the NiO(4 nm) film. The minor loop of the Fe-Ni layer is shown in the inset of (b). The orientation schemes assume that the Fe-Ni magnetization is either parallel (a) or perpendicular (b) to the  $\mathbf{c}$  axis; the horizontal axis is always parallel to the  $\mathbf{y}$  axis of the light coordinate system.

asymmetric shape, which means that the coupling between FM layers is not perfectly at  $90^\circ$  in zero field. No exchange bias field effect has been seen here at room temperature. This is due to the very small NiO grain size ( $\sim 7$  nm), which results from the deposition at oblique incidence, and leads to an inefficient pinning of the NiO spin lattice.<sup>12</sup>

In order to have a more accurate determination of the relative orientation of the magnetization in the Co and Fe-Ni layers, we performed LMOKE measurements on the NiO(4 nm) film in transverse ( $\parallel \mathbf{x}$ ) field (Fig. 1), applied along the  $\mathbf{c}$  axis, or slightly misoriented from it by an angle  $\eta$  (Fig. 3). For  $\mathbf{H}$  strictly applied along the  $\mathbf{c}$  axis ( $\eta = 0$ ), the field-induced magnetization component  $M_x$  of the Co layer must be always zero; as expected in that case, no remnant of a Co loop at high field is observed [Fig. 3(a)]. The remaining effect comes only from the Fe-Ni layer. In the case of an ideal  $90^\circ$  magnetic coupling between the two FM layers in zero field, no hysteresis or complex field behavior is expected for the Fe-Ni layer because of the compensation between domains with opposite magnetization along the  $\mathbf{y}$  axis after reaching saturation. The inversion of sign of the LMOKE loop related to the inversion of the field variation [Fig. 3(a)] means that the easy axis makes a fixed angle  $\theta$  with the normal to the  $\mathbf{c}$  axis. Jumps in LMOKE are then expected for opposite fields  $H_j = \pm H_C / \sin \theta$ .  $H_C = 8$  Oe is the Fe-Ni coercivity measured along the normal to the  $\mathbf{c}$  axis. In

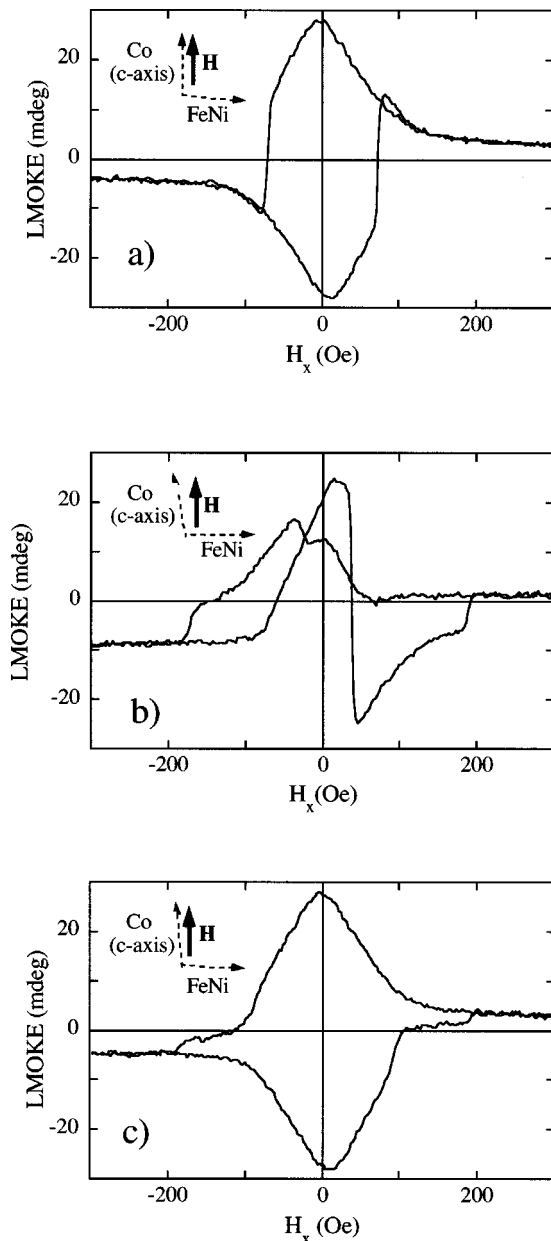


FIG. 3. LMOKE loops of the NiO(4 nm) film in transverse field ( $\mathbf{H}\parallel\mathbf{x}$ ). (a)  $\mathbf{H}$  rigorously applied along the  $\mathbf{c}$  axis ( $\eta=0^\circ$ ), and slightly misoriented by angles (b) ( $\eta=5^\circ$ ), (c) ( $\eta=2^\circ$ ), with respect to  $\mathbf{c}$ . The orientation schemes assume that the orientation of the Fe-Ni magnetization with respect to the  $\mathbf{c}$  axis is a little larger than  $90^\circ$ .

the present case  $H_j \approx 80$  Oe [Fig. 3(a)], so that one deduces  $\theta \approx 6^\circ \pm 1^\circ$ . We effectively found an erratic field-induced magnetic behavior for transverse LMOKE measurements when  $\eta$  is fixed to  $5^\circ \pm 1^\circ$  [Fig. 3(b)], i.e., when the field becomes strictly perpendicular to the equilibrium Fe-Ni magnetization in zero field.<sup>24</sup> When the misorientation angle  $\eta$  is smaller than  $2^\circ$ , the predicted value for  $H_j$  exceeds the maximum applied field value, and no jump in Fe-Ni magnetization is observed, as depicted in Fig. 3(c).

As already mentioned, MSHG can be studied in four distinct optical configurations depending on the polarization ( $s$

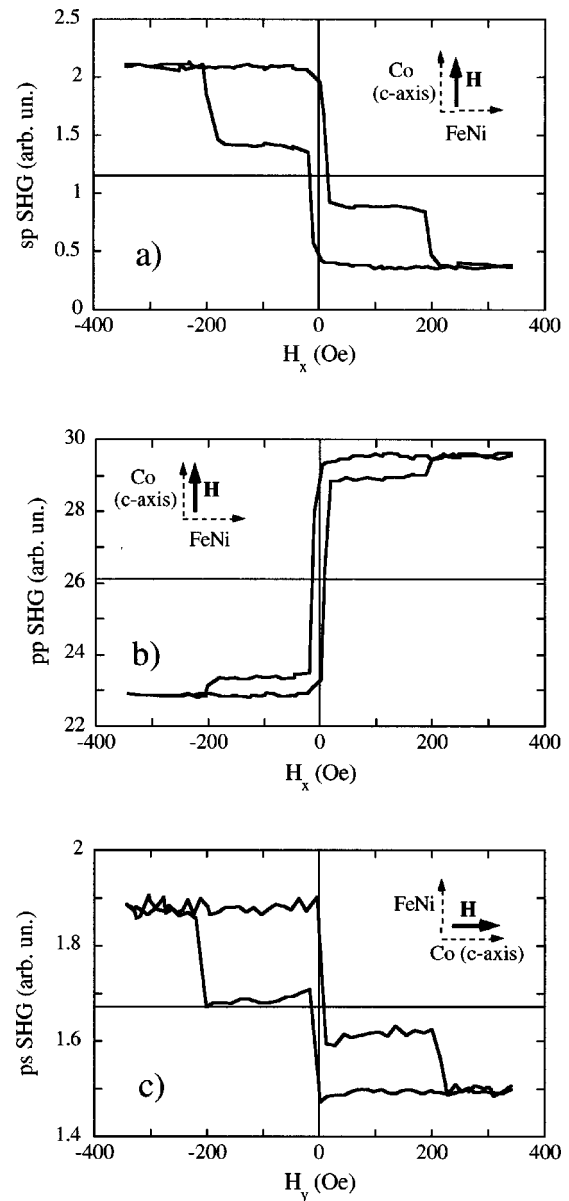


FIG. 4. MSHG hysteresis loops of the NiO(8 nm) film, measured in transverse field ( $\mathbf{H}\parallel\mathbf{x}$  and  $\parallel\mathbf{c}$ ) for (a)  $s_{in}p_{out}$  and (b)  $p_{in}s_{out}$  optical configurations, and (c) in longitudinal field ( $\mathbf{H}\parallel\mathbf{y}$  and  $\parallel\mathbf{c}$ ) in the  $p_{in}s_{out}$  optical configuration. To simplify, the schemes assume that the Fe-Ni magnetization is at  $90^\circ$  from the  $\mathbf{c}$  axis.

or  $p$ ) of the incoming (in) and outgoing (out) beams (Fig. 1). These configurations test in-plane magnetization components.<sup>2</sup> In order to measure MSHG hysteresis loops, we used an experimental setup with a mode-locked Ti: sapphire laser giving 100-fs light pulses centered at 800 nm, and working at a repetition rate of 86 MHz.<sup>25</sup> The average light power on the sample surface was 50 mW, with a focused beam size of 30–40  $\mu\text{m}$ . The angle of incidence was  $45^\circ$ . MSHG hysteresis loops of our magnetic film structure exhibit obviously different shapes compared to the considered light polarization configuration. As discussed below, these differences are mainly related to the MSHG in-depth sensitivity.

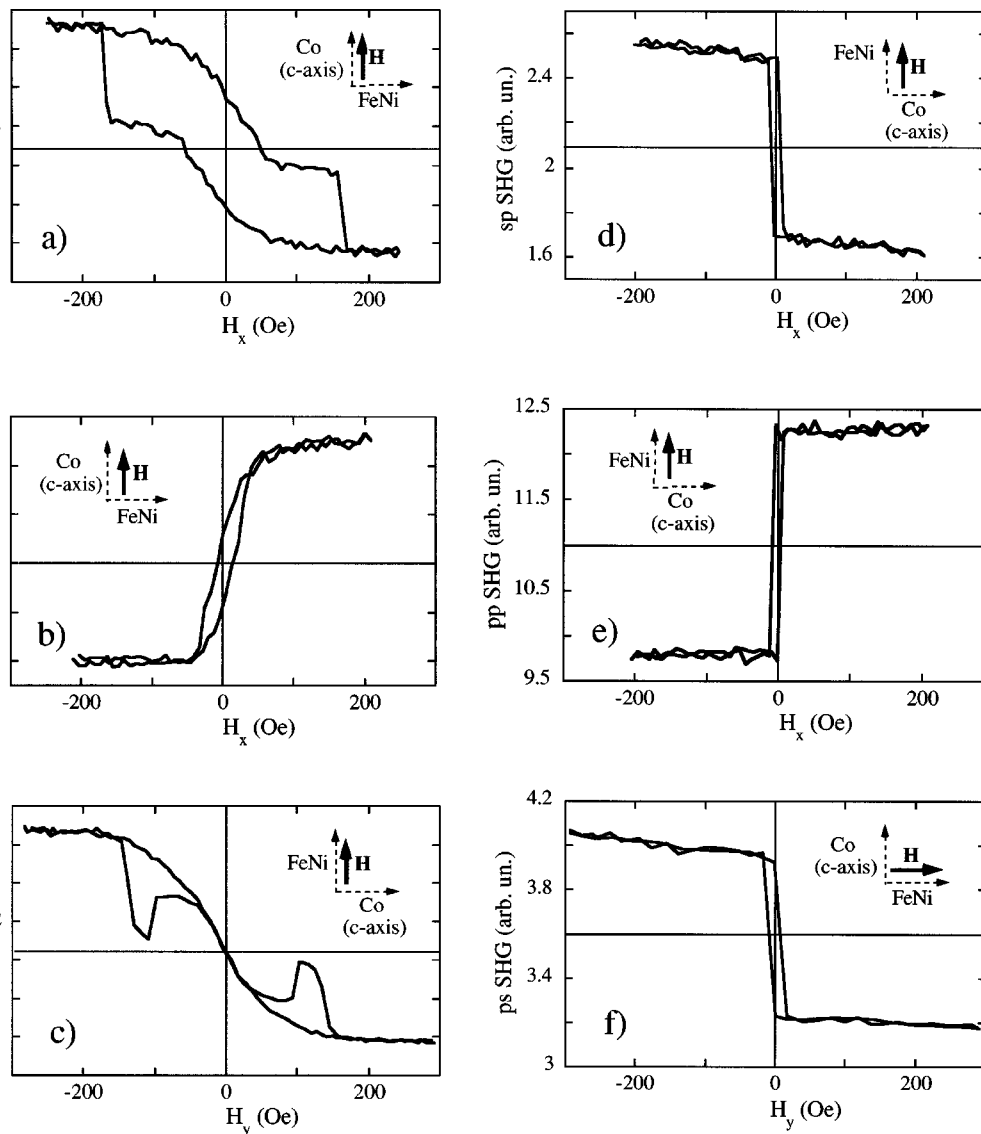


FIG. 5. MSHG hysteresis loops of the NiO(4 nm) film, measured in transverse field ( $\mathbf{H} \parallel \mathbf{x}$  and  $\perp \mathbf{c}$ ) for (a)  $s_{in}p_{out}$  and (b)  $p_{in}p_{out}$  optical configurations, and (c) in longitudinal field ( $\mathbf{H} \parallel \mathbf{y}$  and  $\parallel \mathbf{c}$ ) in the  $p_{in}s_{out}$  optical configuration. Similar data are shown in (d)–(f) when  $\mathbf{H} \perp \mathbf{c}$ . To simplify, the schemes assume that the Fe-Ni magnetization is at  $90^\circ$  from the  $\mathbf{c}$  axis.

Our MSHG results for the NiO(8 nm) and NiO(4 nm) film are depicted in Figs. 4 and 5. The  $s_{in}p_{out}$  MSHG hysteresis loops, measured in a transverse field ( $\mathbf{H} \parallel \mathbf{x}$ ) applied along the  $\mathbf{c}$  axis, are shown in Figs. 4(a) and 5(a) for the NiO(8 nm) and NiO(4 nm) film, respectively. The shape of these  $s_{in}p_{out}$  MSHG hysteresis loops is quite similar to that of LMOKE loops [Figs. 2(a) and 2(b)]. Note that MSHG is supposed to be sensitive only to the magnetization of the interfaces of the Co and Fe-Ni layers, while LMOKE probes the magnetization of the layers themselves. At this stage, the similarity between the above  $s_{in}p_{out}$  MSHG and LMOKE loops tends to demonstrate that either the coupling between Co and Fe-Ni interfaces is closely similar to that existing between FM layers, or the *optically active* MSHG region expands around interfaces.

The  $p_{in}p_{out}$  MSHG hysteresis loop, measured in a transverse ( $\mathbf{H} \parallel \mathbf{x}$ ) field still applied along the  $\mathbf{c}$  axis, is dominantly sensitive to Fe-Ni interfaces in both samples [Figs. 4(b) and

5(b)]. For the NiO(8 nm) film, a rather large  $p_{in}p_{out}$  MSHG effect is observed. It comes mainly from the Fe-Ni interfaces since the amplitude of the Co loop is rather weak here [Fig. 4(b)]. For the NiO(4 nm) film, only a quasiuniform rotation of the field-induced magnetization at Fe-Ni interfaces can be measured; it can be compared with the LMOKE Fe-Ni minor loop [inset of Fig. 2(b)]. The sharp selectivity to buried Fe-Ni interfaces in both samples is clearly related to the in-depth sensitivity of MSHG in this particular  $p_{in}p_{out}$  optical configuration; we will return to this point later.

In the  $p_{in}s_{out}$  MSHG configuration with  $\mathbf{H} \parallel \mathbf{x}$  and  $\mathbf{c}$ , the resulting loop for the NiO(8 nm) film [Fig. 4(c)] is still quite comparable to that obtained in LMOKE [Fig. 2(a)]. The result is more surprising for the NiO(4 nm) film, where two opposite jumps are observed at  $H_C \sim 120$  and  $170$  Oe [Fig. 5(c)]. The magnetization jump at the higher field is obviously due to the Co layer, while the occurrence of the other new jump will be discussed later.

Another set of MSHG hysteresis loops have been still measured in the same optical  $s_{\text{in}}p_{\text{out}}$ ,  $p_{\text{in}}p_{\text{out}}$ , and  $p_{\text{in}}s_{\text{out}}$  configurations, but with films rotated by  $90^\circ$  around their normal axis, i.e., for a magnetic field applied perpendicular to the  $\mathbf{c}$  axis [Figs. 5(d)–5(f)]. Results are only given for NiO(4 nm), for which MSHG calculations have been performed. Considering the relatively weak value of the maximum applied field value in this case ( $<300$  Oe), only minor Fe-Ni loops are measured. Thus, the switching of the Co layer cannot be seen below 300 Oe, but a progressive rotation of the Co spins towards the field direction might be seen. This is exactly what we measured in LMOKE in the same field range (not shown here). The MOKE loop shape ( $H_{\text{max}}=200$  Oe) is comparable to that found in  $s_{\text{in}}p_{\text{out}}$  MSHG [Fig. 5(d)], i.e., a narrow highly square Fe-Ni loop with low coercivity ( $H_C=8$  Oe) at low field, superimposed to a reversible signal due to Co spins, proportional to  $H$ . The progressive rotation of the magnetization at Co interfaces, when  $\mathbf{H} \perp \mathbf{c}$ , is only revealed in  $s_{\text{in}}p_{\text{out}}$  and  $p_{\text{in}}s_{\text{out}}$  MSHG configurations, as indicated by the observed slope for  $H > H_C$ . Again, as for  $\mathbf{H} \parallel \mathbf{c}$ ,  $p_{\text{in}}p_{\text{out}}$  MSHG is not sensitive to Co layer interfaces since above 10 Oe the signal stays constant. All MSHG data confirm that the exchange coupling between the Co and Fe-Ni interfaces is still close to  $90^\circ$  for the NiO(4 nm) film and weakly ferromagnetic for the NiO(8 nm) film.

## V. INTERPRETATION AND DISCUSSION

We propose to determine the in-depth sensitivity of MSHG and its selectivity to interfaces in the film structure defined in Sec. III. More precisely, it is important to understand the relative efficiency of MSHG for different magnetic interfaces and for various optical configurations. Particularly relevant are the determinations of the selection rules of the emitted radiation at frequency  $2\omega$ , and first the magnitude of the electric field at frequency  $\omega$  at each interface of the multilayer. To simplify the presentation, and without losing generality, further calculations and discussions will be essentially limited to the NiO(4 nm) film structure.

The in-depth profile of the modulus of the components of the electric field at frequency  $\omega$  is calculated for the above studied structure and for an incoming light penetrating the structure from the CoO side (Fig. 6). The continuity of the normal component of the electric induction  $\mathbf{D}^{(\omega)}$  through the  $\nu$ th interface implies the relation  $\epsilon_{0,\nu}^{(\omega)} E_{z,\nu}^{(\omega)} = \epsilon_{0,\nu+1}^{(\omega)} E_{z,\nu+1}^{(\omega)}$ , where  $\epsilon_{0,\nu}^{(\omega)}$  represents the diagonal permittivity matrix element of the  $\nu$ th layer. Thus, the normal electric field component  $|E_z^{(\omega)}|$  can exhibit strong discontinuities at interfaces. Since the ratio between the diagonal permittivity elements for a metal (Co) and an insulating material (CoO or NiO) is rather large, one expects a huge jump of  $|E_z^{(\omega)}|$  at both sides of the Co layer (Fig. 6). In contrast, due to the continuity of the tangential components,  $|E_x^{(\omega)}|$  and  $|E_y^{(\omega)}|$ , of the electric field across the interfaces, the in-depth profiles of these last quantities vary continuously through the interfaces, and their amplitudes are smoothly decreasing when light is penetrating deeper inside the structure (Fig. 6). Note also that in metals, the amplitude of the electric field component  $|E_z^{(\omega)}|$  is smaller

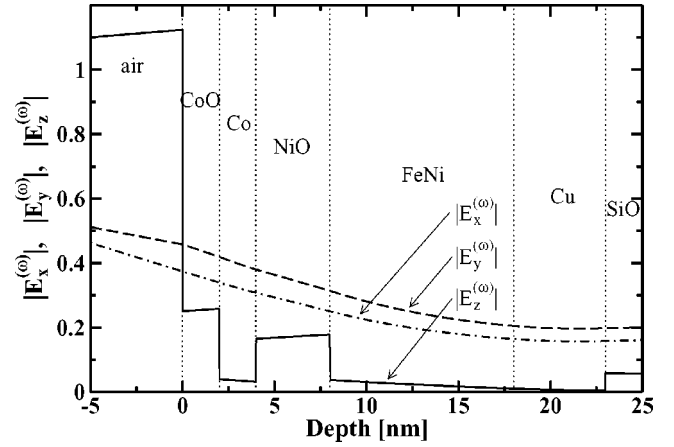


FIG. 6. In-depth profile of the modulus of the components of the electric field of the electromagnetic radiation for  $|E_x^{(\omega)}|$ ,  $|E_y^{(\omega)}|$ , and  $|E_z^{(\omega)}|$  for the CoO(2 nm)/Co(2 nm)/NiO(4 nm)/Ni-Fe(10 nm)/Cu(5 nm)/SiO<sub>2</sub>(100 nm)/Si film structure. The successive interface positions are noted by vertical dashed lines. The values of incoming electric amplitudes are assumed to be  $\epsilon_{0,s}^{(\omega)}=1$  or  $\epsilon_{0,p}^{(\omega)}=1$ ; the incidence angle is  $\varphi=45^\circ$  and the photon energy  $E=1.55$  eV.

than  $|E_x^{(\omega)}|$  and  $|E_y^{(\omega)}|$  because of the large refractive indices of metals. As a consequence, the light propagates in metallic layers in a direction nearly perpendicular to interfaces of the multilayer structure. Finally, note that variation of light intensity inside air is due to interference between incoming and reflected light beams, an effect observable also with a simple mirror. The variation of  $\mathbf{E}_\nu^{(\omega)}$  over a larger distance in the air would follow a sine function.

The values of the electric field  $\mathbf{E}_\nu^{(\omega)}$  at the interface  $\nu$  can be identified as incoming Fresnel coefficients (i.e., the  $\mathbf{X}_\nu^{(\omega)}$  elements) when the incident electric field amplitudes are taken as unity [see Eq. (1)]. The real and imaginary parts of the incoming Fresnel coefficients in the studied structure are presented in Fig. 7. Going deeper and deeper in the structure, the amplitude of all electric field components on successive interfaces decrease monotonically, due to both damping and reflections inside the structure. At the same time, the phases of the  $E_x^{(\omega)}$  and  $E_y^{(\omega)}$  components of the electric field (i.e.,  $X_{xs,\nu}^{(\omega)}$  and  $X_{yp,\nu}^{(\omega)}$  elements) vary continuously.

The situation is quite different for the emitted light at frequency  $2\omega$ . Figure 8 represents the real and imaginary parts of generalized outgoing Fresnel coefficients (i.e.,  $\mathbf{Z}_\nu^{(2\omega)}$  elements) [see Eq. (3)]. The radiated amplitude of the normal component  $\mu_z^{(2\omega)}$  (provided by  $Z_{pz,\nu}^{(2\omega)}$ ) is about twice more efficient than that of in-plane  $\mu_x^{(2\omega)}$  and  $\mu_y^{(2\omega)}$  components (provided by  $Z_{xs,\nu}^{(2\omega)}$  and  $Z_{py,\nu}^{(2\omega)}$ ). Furthermore, both the amplitude and phase of  $\mu_x^{(2\omega)}$  and  $\mu_y^{(2\omega)}$  decrease monotonically with increasing in-depth location of the radiating dipole located in the close vicinity of interfaces. In the case of our particular structure, the radiation emitted by  $\mu_x^{(2\omega)}$  or  $\mu_y^{(2\omega)}$  unitary dipoles on either the CoO/Co or Fe-Ni/Cu interface differs only by about 30%. In the case of a  $\mu_z^{(2\omega)}$  radiated component (provided by  $Z_{pz,\nu}^{(2\omega)}$ ), the situation is not so straightforward, but there is still a relatively weak dependence of the dipole radiation with its in-depth location. Thus,

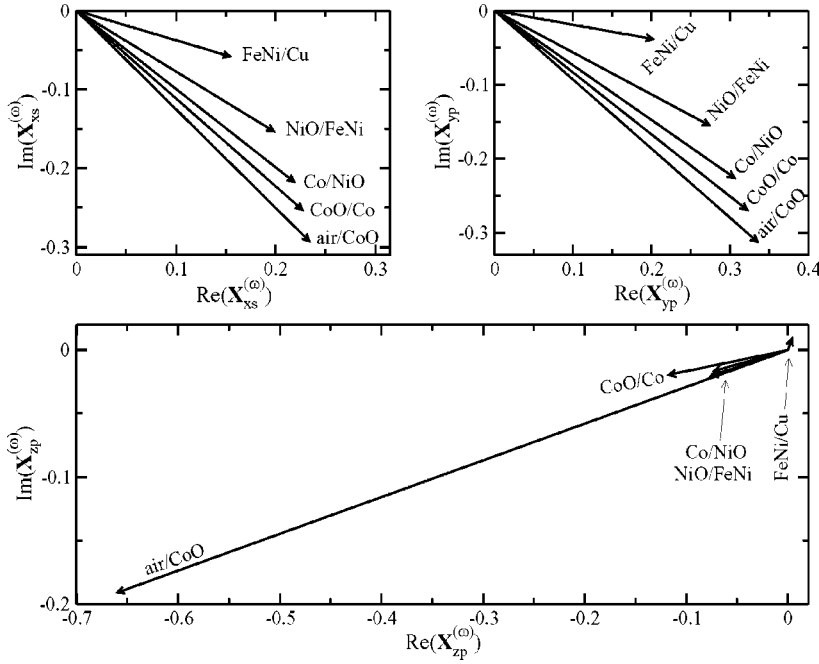


FIG. 7. Complex representation of the non-zero elements of the  $\mathbf{X}^{(\omega)}$  matrix [defined by Eq. (1)] for the CoO(2 nm)/Co(2 nm)/NiO(4 nm)/Ni-Fe(10 nm)/Cu(5 nm)/SiO<sub>2</sub>(100nm)/Si film structure. The calculations are done for an incidence angle  $\varphi=45^\circ$ , and for  $E=1.55$  eV.

Fig. 8 demonstrates that the dipole radiation itself is not very in-depth sensitive, and thus the experimentally observed *in-depth selectivity of the MSHG radiation is essentially determined by the profile of the incident electrical field  $\mathbf{E}^{(\omega)}$* .

Let us consider first the  $s_{in}p_{out}$  MSHG in a transverse field applied along the  $\mathbf{c}$  easy anisotropy axis of the Co layer ( $\mathbf{H} \parallel \mathbf{x}, \mathbf{c}$ ). MSHG, only sensitive to the transverse magnetization component  $M_x$  (Table I), is then proportional to  $\chi_{yxx}^{(m)} (E_x^{(\omega)})^2$ . Only one magnetic term per magnetic interface is concerned in Eq. (6). As it can be seen in Fig. 6, the  $|E_x^{(\omega)}|$  field modulus has appreciable values at all interfaces, but shows only a slow decrease with increasing in-depth location of interfaces. Therefore, the resulting MSHG hysteresis loops, measured in this configuration, must contain contributions from all magnetic interfaces and are certainly not very selective to particular interfaces. Actually, this is confirmed by the shape of the resulting hysteresis loop [Figs. 4(a) and 5(a)], which clearly involves magnetic contributions from all interfaces with Co and Fe-Ni, i.e., CoO/Co, Co/NiO, NiO/Fe-Ni, and Fe-Ni/Cu interfaces are probed. The simi-

ilarity between the transverse  $s_{in}p_{out}$  MSHG [Figs. 4(a) and 5(a)] and LMOKE [Figs. 2(a) and 2(b)] loops is also consistent with the fact that  $s_{in}p_{out}$  MSHG is supposed to probe the magnetization around interfaces over a non-negligible thickness extending into the Co and Ni-Fe layers. The fact that  $s_{in}p_{out}$  MSHG probes a relatively thick ( $\sim 1$  nm) interface region is consistent with predictions of Ref. 16, as already discussed in Sec. II.

The  $s_{in}p_{out}$  MSHG hysteresis loop of the NiO(4 nm) film in a relatively small transverse field ( $\mathbf{H} \parallel \mathbf{x}$ ) (minor loop), but applied now perpendicular to the  $\mathbf{c}$ -axis MSHG [Fig. 5(d)], is the superposition of a square loop due to the Fe-Ni interfaces plus an additional quasilinear field-dependent signal related to the canting of the Co spins. This is still in agreement with a  $90^\circ$  exchange spin coupling between Co and Fe-Ni interfaces. The relative amplitude of  $s_{in}p_{out}$  MSHG due to Co and Fe-Ni interfaces is also consistent with that found for  $\mathbf{H} \parallel \mathbf{c}$ .

In the  $p_{in}p_{out}$  MSHG optical configuration in a transverse field ( $\mathbf{H} \parallel \mathbf{x}, \mathbf{c}$ ), there is no signal variation above 50 Oe [Fig. 4(b)]. MSHG solely comes from the magnetization behavior

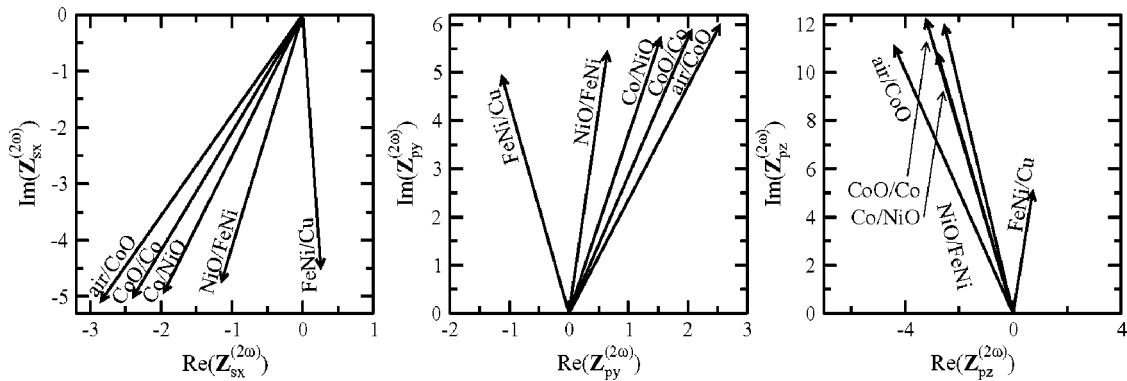


FIG. 8. Complex representation of nonzero generalized outgoing Fresnel coefficients [i.e., elements of  $\mathbf{Z}^{(2\omega)}$ , defined by Eq. (3)] for the same film structure ( $\varphi=45^\circ$ , and  $E=3.1$  eV).

at Fe-Ni interfaces in a field applied at  $\theta=6^\circ$  from the zero-field magnetization equilibrium state of the Fe-Ni layer. As for LMOKE data [inset of Fig. 2(b)], the possible difference in slope of the MSHG signal in positive or negative field larger than 50 Oe and the open hysteresis loop can be explained by this small misalignment angle by  $6^\circ$  of the field. Considering the accuracy of our MSHG experiments, it is difficult to distinguish between the field-induced magnetic behavior for the Fe-Ni interfaces and the Fe-Ni layer itself and to deduce the misalignment angle  $\theta$  in Fe-Ni interfaces from MSHG.

The insensitivity to the Co interfaces is also seen in transverse  $p_{in}p_{out}$  MSHG for  $\mathbf{H} \perp \mathbf{c}$  [Fig. 5(e)]. As expected, only the low-coercivity square loop of Fe-Ni interfaces survives, with no significant field-dependent variation at field higher than 10 Oe.

Looking at Table I,  $p_{in}p_{out}$  MSHG is only sensitive to the transverse component  $M_x$  of the magnetization. The MSHG intensity is then theoretically related to  $\mu_y^{(2\omega)} = \chi_{yyy}^{(m)} (E_y^{(\omega)})^2 + \chi_{yzz}^{(m)} (E_z^{(\omega)})^2$  and  $\mu_z^{(2\omega)} = \chi_{zzy}^{(m)} (E_z^{(\omega)} E_y^{(\omega)})$  terms. Three susceptibility elements and two electric field components are then involved. Experimentally, we essentially measure loops related to Fe-Ni interfaces [Figs. 4(b) and 5(b)], in spite of the fact that they are localized deeper in the structure than the Co layer. This is closely linked with the in-depth sensitivity profile of  $E_z^{(\omega)}$  (Fig. 6). As the Co layer is surrounded by two oxide layers (CoO and NiO), with nearly similar optical properties, the  $E_z^{(\omega)}$  discontinuity at each CoO/Co and Co/NiO interface has comparable size. The similarity of both interfaces is demonstrated from cross-section transmission electron microscopy and EXAFS measurements that have also shown that an ultrathin ( $\sim 0.3$  nm) nonmagnetic oxidized CoO or CoNiO layer is present at the Co/NiO interface.<sup>12</sup> Hence, since both interfaces are optically very similar, the associated  $\chi$  values can be assumed to be similar as well. Thus, the MSHG signal generated by these two interfaces has nearly the same amplitude, but with a difference in phase shift equal to  $\pi$ . So, the two MSHG contributions for these Co interfaces are supposed to cancel each other. In other words, MSHG for these two mirrored interfaces vanishes since a full symmetry with respect to the spacing medium is preserved. On the other hand, the Fe-Ni layer is surrounded by one oxide (NiO) and one metallic (Cu) layer, giving an inherent large change of the optical properties at both sides of the interface. Since the jump in  $|E_z^{(\omega)}|$  is far larger for the NiO/Fe-Ni interface than for the Fe-Ni/Cu one (Fig. 6), the source of MSHG comes predominantly from the NiO/Fe-Ni interface. This also means that we are mainly sensitive to terms related to  $E_z^{(\omega)}$ , and the term  $\mu_y^{(\omega)} = \chi_{yyy}^{(m)} (E_y^{(\omega)})^2$  must vanish for the NiO/Fe-Ni interface. Thus, only two terms survive,  $\mu_y^{(\omega)} = \chi_{yzz}^{(m)} (E_z^{(\omega)})^2$  and  $\mu_z^{(2\omega)} = \chi_{zzy}^{(m)} \times (E_z^{(\omega)} E_y^{(\omega)})$ . From symmetry arguments,  $\chi_{xzz}^{(m)} = -\chi_{yzz}^{(m)}$  (Table II) and, as shown below for the  $p_{in}p_{out}$  configuration,  $\chi_{xzz}^{(m)}$  is found to be negligible. Thus, the  $\mu_y^{(\omega)} = \chi_{yzz}^{(m)} (E_z^{(\omega)})^2$  term can be considered small as well. In conclusion, the hysteresis loop measured in transverse  $p_{in}p_{out}$  configuration [Figs. 4(b) and 5(b)] probes selectively the NiO/Fe-Ni interface through the dominant  $\chi_{zzy}^{(m)} (E_z^{(\omega)} E_y^{(\omega)})$  term.

As given in Table I, no nonmagnetic term is predicted for pure  $s_{in}s_{out}$  or  $p_{in}s_{out}$  optical configurations. So, since MSHG depends on products of nonmagnetic and magnetic terms, the analyzer must be slightly misoriented by an angle  $\gamma$  from a pure  $s$  orientation to restore a nonmagnetic component originating from a  $p_{out}$  optical configuration.

For the so-called  $s_{in}s_{out}$  configuration, this allows us to restore a nonmagnetic component coming from the  $s_{in}p_{out}$  configuration (Table I), and thus to be sensitive to the longitudinal  $M_y$  component of the magnetization. However, in this case, no significant MSHG has been experimentally detected, which means that  $\chi_{xxx}^{(m)}$  is small for all magnetic interfaces. This is in agreement with our previous discussion on  $p_{in}p_{out}$  MSHG, mentioning that  $\chi_{yyy}^{(m)}$  is negligible, and considering that  $\chi_{xxx}^{(m)} = -\chi_{yyy}^{(m)}$  (Table II).

In the  $p_{in}s_{out}$  case, the analyzer has to be still crossed by a small angle  $\gamma$  ( $\gamma \sim 10^\circ$ ) to restore a nonmagnetic component related to  $p_{in}p_{out}$ . Then,  $p_{in}s_{out}$  MSHG, related to the longitudinal  $M_y$  component, can be detected. More precisely, one can have access both to a longitudinal  $p_{in}s_{out}$  magnetic contribution with amplitude proportionnal to  $M_y \sin \gamma \cos \gamma$ , and a transverse  $p_{in}p_{out}$  component proportional to  $M_x \sin^2 \gamma$ . Their relative magnitude depends not only on the analyzer misorientation  $\gamma$ , but also on the involved susceptibility elements and electrical fields. The longitudinal  $p_{in}s_{out}$  magnetic contribution is determined by  $\mu_x^{(2\omega)} = \chi_{xyy}^{(m)} (E_y^{(\omega)})^2 + \chi_{xzz}^{(m)} (E_z^{(\omega)})^2$  (Table I). As presented in Figs. 5(c) and 5(f), the hysteresis loops, measured in a field parallel or perpendicular to the  $\mathbf{c}$  axis, contain contributions from both Co and Fe-Ni interfaces. Thus,  $p_{in}s_{out}$  MSHG is not very in-depth selective, leading to a small in-depth resolved term  $\chi_{xzz}^{(m)} (E_z^{(\omega)})^2$ . The term  $\chi_{xyy}^{(m)} (E_y^{(\omega)})^2$  consequently has a dominant role. Recall that this proved the smallness of  $\chi_{xzz}^{(m)} (E_z^{(\omega)})^2 = -\chi_{yzz}^{(m)} (E_z^{(\omega)})^2$  (Table II), as it has been already used to determine the dominant term for  $p_{in}p_{out}$  MSHG.

The experimental  $p_{in}s_{out}$  MSHG data obtained for the NiO(8 nm) film in  $\mathbf{H} \parallel \mathbf{c}$  is the superposition of two loops linked to the magnetic state of the Co and Fe-Ni interfaces [Fig. 4(c)]. Roughly speaking, it looks again quite similar to LMOKE, which means that  $p_{in}s_{out}$  MSHG relates to the longitudinal  $M_y$  component of the magnetization.

In counterpart,  $p_{in}s_{out}$  MSHG gives a complex loop for the NiO(4 nm) film that can be interpreted by considering the two above-discussed contributions that always involve a  $p_{in}p_{out}$  nonmagnetic term, coupled with either  $p_{in}s_{out}$  or  $p_{in}p_{out}$  magnetic terms (Table I). The  $p_{in}s_{out}$  magnetic contribution then tests the  $M_y$  component of the magnetization of each interface, while the  $p_{in}p_{out}$  one gives access to  $M_x$ . So, the resulting  $p_{in}s_{out}$  MSHG loop can be decomposed into (i) signals proportional to  $M_y$  of Co and Fe-Ni interfaces, i.e., a square loop related to Co interfaces plus S-shaped field variations related to Fe-Ni interfaces, and (ii) signals proportionnal to  $M_x$  of Fe-Ni interfaces. The loops corresponding to (i) are quite similar to LMOKE or  $s_{in}p_{out}$  MSHG. In a perfect case, for Fe-Ni spins oriented perpendicular to the  $\mathbf{c}$  axis, the contribution (ii) must vary monotonically from a maximum for  $H=0$  to zero in large fields, for LMOKE measured in a transverse field (Fig. 3). As found in simulations,<sup>12</sup> and suggested above, if the spin orientation in the Fe-Ni/NiO inter-

face is not exactly normal to the  $\mathbf{c}$  axis (but misoriented by the angle  $\theta$ ), one can predict an associated  $M_x(H)$  loop with two opposite large symmetric jumps. They are associated with abrupt field-induced spin reorientations along the zero-field equilibrium Fe-Ni magnetization axis from one direction to the opposite. Such an effect was already seen in LMOKE measured in a transverse field (Fig. 3).

In the case of the longitudinal  $p_{in}p_{out}$  MSHG loop measured in a field perpendicular to  $\mathbf{c}$  [Fig. 5(c)], the field-induced transverse magnetization  $M_x$  of the Fe-Ni layer and of related interfaces is always zero, so no additional  $p_{in}p_{out}$  MSHG term is expected.

Up to now, we have not considered SHG coming from the centrosymmetric antiferromagnetic NiO layer,<sup>19,21</sup> especially in the  $p_{in}s_{out}$  configuration. This effect must be only related to the square of the sublattice magnetization,<sup>26</sup> which does not change sign with the applied magnetic field. Since the measured magnetically induced SHG effects are odd with field, we exclude any second-harmonic contribution of the NiO layer in the observed hysteresis loops. Moreover, since  $K_{NiO} = 4 \times 10^4$  erg/cm<sup>3</sup> is far from being negligible, the antiferromagnetic spin-flop reorientation from the  $\mathbf{c}$  axis to its normal cannot occur before the magnetization switching of the Co layer.

## VI. CONCLUSION

The in-depth selectivity of MSHG in the Co/NiO/Fe-Ni thin film structure has been investigated. We experimentally proved that  $p_{in}p_{out}$  MSHG is very selective to specific interfaces, whereas the  $p_{in}s_{out}$  and  $s_{in}p_{out}$  MSHG configurations are selective to all interfaces. The depth location of the  $2\omega$ -radiating dipole has only a small impact on the MSHG depth selectivity. The profile of the electric field  $\mathbf{E}^{(\omega)}$  of the incident light beam is shown to govern this selectivity. Profiles of electrical field components  $E_x^{(\omega)}$ ,  $E_y^{(\omega)}$  are continuous through the multilayer, although  $E_z^{(\omega)}$  varies discontinuously at interfaces. Hence, the depth selectivity is attributed to the  $E_z^{(\omega)}$  component. Symmetry arguments (Tables I and II) give

the principal contributions for each MSHG configuration in our case. They are  $\mu_z^{(2\omega)} = \chi_{zzy}^{(m)} E_y^{(\omega)} E_z^{(\omega)}$  for  $p_{in}p_{out}$  MSHG,  $\mu_x^{(2\omega)} = \chi_{xyy}^{(m)} (E_y^{(\omega)})^2$  for  $p_{in}s_{out}$  MSHG and  $\mu_y^{(2\omega)} = \chi_{yxx}^{(m)} (E_x^{(\omega)})^2$  for  $s_{in}p_{out}$  MSHG. We can generalize our results and conclude that the  $p_{in}p_{out}$  MSHG configuration is mainly sensitive to the interfaces of dielectric/FM or air/FM type and not to metal/FM interfaces, FM being a ferromagnetic metal. This is due to a large discontinuity of  $E_z$  at dielectric/FM or air/FM interfaces, originating from the relatively small refractivity indices of air and dielectrics as compared to metals. On the other hand,  $s_{in}p_{out}$  and  $p_{in}s_{out}$  configurations depend on all interfaces.

In the  $p_{in}s_{out}$  MSHG configuration, we have observed a superimposed hysteresis loop that is assigned to the transverse magnetization of the Fe-Ni/NiO interface, since the misorientation of the analyzer allows to check simultaneously the two in-plane magnetization components. In the NiO(4 nm) film, we deduce that the orientation of the magnetization at the Fe-Ni/NiO interface (by MSHG) and inside the Fe-Ni layer (by LMOKE) are misoriented by several degrees from the normal to the  $\mathbf{c}$  axis. Unfortunately, considering the limited accuracy of MSHG data, it is difficult to demonstrate if this misorientation angle is strictly the same in the Fe-Ni layer and at its interface with the NiO layer.

As stated in Refs. 16 and 17,  $\mu_z^{(2\omega)}$  probes a much more localized interface region ( $\sim 0.1$  nm) than  $\mu_x^{(2\omega)}$  or  $\mu_y^{(2\omega)}$  ( $\sim 1$  nm). The inspection of dominant terms in Table I indicates that it corresponds to the fact that  $p_{in}p_{out}$  MSHG sharply probes interfaces while  $s_{in}p_{out}$  and  $p_{in}s_{out}$  MSHG are also influenced by the magnetization state inside ultrathin layers.

## ACKNOWLEDGMENTS

J.H. has received support from the NOMOKE Contract No. HPMT-CT-2000-00066 from the European Community and from a grant of the French Ministère des Affaires Étrangères. The visits of L.C. Sampaio and F. Garcia were financially supported by CNPq/Brazil.

\*Present address: Centro Brasileiro de Pesquisas Físicas/MCT, Rio de Janeiro, Brazil.

†Present address: Frontier Research System, The Institute of Physical and Chemical Research (RIKEN), 2-1 Hirosawa, Wako, Saitama 351-0198, Japan.

<sup>1</sup>*The Principles of Nonlinear Optics*, edited by Y. R. Shen (Wiley, New York, 1984).

<sup>2</sup>*Non-linear Optics in Metals*, International Series of Monographs on Physics, edited by K.-H. Benneman (Oxford University Press, Oxford, 1998).

<sup>3</sup>Ru-Pin Pan, H. D. Wei, and Y. R. Shen, Phys. Rev. B **39**, 1229 (1989).

<sup>4</sup>W. Hübner, Phys. Rev. B **42**, 11553 (1990).

<sup>5</sup>A. Kirilyuk, J. Phys. D **35**, R189 (2002).

<sup>6</sup>J. Ferré, in *Magnetism and Synchrotron Radiation*, Lecture Notes

in Physics, edited by E. Beaurepaire *et al.* (Springer, Heidelberg, 2001), p. 316.

<sup>7</sup>J. Hamrle, J. Ferré, M. Nyvlt, and S. Visnovsky, Phys. Rev. B **66**, 224423 (2002).

<sup>8</sup>G. Spiering, V. Koustos, H. Wierenga, M. Pins, D. Abraham, and T. Rasing, J. Magn. Magn. Mater. **121**, 109 (1993); H. Wierenga, Ph.D. thesis, Nijmegen (1996).

<sup>9</sup>R. Atkinson and N. F. Kubrakov, Appl. Phys. B: Lasers Opt. **74**, 697 (2002).

<sup>10</sup>L. C. Sampaio, A. Mougin, J. Ferré, P. Georges, A. Brun, H. Bernas, S. Poppe, T. Mewes, J. Fassbender, and B. Hillebrands, Europhys. Lett. **63**, 819 (2003).

<sup>11</sup>Y. Z. Wu, R. Vollmer, H. Regensburger, X.-F. Jin, and J. Kirshner, Phys. Rev. B **63**, 054401 (2001).

<sup>12</sup>J. Camarero, Y. Pennec, J. Vogel, M. Bonfim, S. Pizzini, F. Ernult,

- F. Fettar, F. Garcia, F. Lançon, L. Billard, B. Dieny, A. Tagliaferri, and N. B. Brookes, *Phys. Rev. Lett.* **91**, 027201 (2003); F. Ernult, Ph.D. thesis, Grenoble (2002).
- <sup>13</sup>J. Zak, E. R. Moog, C. Liu, and S. D. Bader, *J. Magn. Magn. Mater.* **88**, L261 (1990).
- <sup>14</sup>H. A. Wierenga, M. W. J. Pins, D. L. Abraham, and Th. Rasing, *Phys. Rev. B* **50**, 1282 (1994); H. A. Wierenga, M. W. J. Pins, and Th. Rasing, *Physica B* **204**, 281 (1995).
- <sup>15</sup>J. Hamrle, L. Polerecky, and J. Ferré, *Phys. Rev. B* **67**, 155411 (2003); J. Hamrle, Ph.D. thesis (<http://tel.ccsd.cnrs.fr/>).
- <sup>16</sup>A. Petukhov and A. Liebsch, *Surf. Sci.* **334**, 195 (1995).
- <sup>17</sup>J. Güdde, J. Hohlfeld, and E. Matthias, *Appl. Phys. B: Lasers Opt.* **74**, 691 (2002).
- <sup>18</sup>R. Atkinson and N. Kubrakov, *Phys. Rev. B* **65**, 014432 (2002).
- <sup>19</sup>A. Dähn, W. Hübner, and K. H. Bennemann, *Phys. Rev. Lett.* **77**, 3929 (1996).
- <sup>20</sup>F. Y. Yang and C. L. Chien, *Phys. Rev. Lett.* **85**, 2597 (2000).
- <sup>21</sup>O. Zaharko, P. M. Oppeneer, H. Grimmer, M. Horisberger, H.-Ch Mertins, D. Abramsohn, F. Schäfers, A. Bill, and H.-B. Braun, *Phys. Rev. B* **66**, 134406 (2002).
- <sup>22</sup>P. A.A. van der Heijden, C. H. W. Swüste, W. J. M. de Jonge, J. M. Gaines, J. T. W. M. van Eemeren, and K. M. Schep, *Phys. Rev. Lett.* **82**, 1020 (1999).
- <sup>23</sup>K. Sato, *Jpn. J. Appl. Phys.* **20**, 2403 (1981).
- <sup>24</sup>A. Stankiewicz, A. Maziewski, J. Ferré, and V. Grolier, *Appl. Phys. Lett.* **74**, 2519 (1999).
- <sup>25</sup>V. V. Pavlov, I. Ferré, P. Meyer, G. Tessier, P. Georges, A. Brun, P. Beauvillain, and V. Mathet, *J. Phys.: Condens. Matter* **13**, 9867 (2001).
- <sup>26</sup>M. Fiebig, D. Fröhlich, Th. Lottermoser, V. V. Pavlov, R. V. Pisarev, and H.-J. Weber, *Phys. Rev. Lett.* **87**, 137202 (2001).
- <sup>27</sup>L. C. Sampaio, J. Hamrle, V. V. Pavlov, J. Ferré, P. Georges, A. Brun, H. LeGall, and J. Ben Yousef (unpublished).